JCTC Journal of Chemical Theory and Computation

Article

pubs.acs.org/JCTC

All-Metal Aromaticity: Revisiting the Ring Current Model among Transition Metal Clusters

Zahra Badri,[†,‡] Shubhrodeep Pathak,[§] Heike Fliegl,[∥] Parviz Rashidi-Ranjbar,*[,‡] Radovan Bast,[⊥,#] Radek Marek,[†,▽] Cina Foroutan-Nejad,*[,▽] and Kenneth Ruud*[,○]

[†]CEITEC − Central European Institute of Technology, Masaryk University, Kamenice 5/A4, CZ−62500 Brno, Czech Republic

[‡]School of Chemistry, College of Science, University of Tehran, Tehran, Iran

[§]Raman Center for Atomic, Molecular and Optical Sciences, Indian Association for the Cultivation of Science, Kolkata 700 032, India

[∥]Centre for Theoretical and Computational Chemistry, Department of Chemistry, University of Oslo, P.O. Box 1033, Blindern, N−0315 Oslo, Norway

[⊥]Laboratoire de Chimie et Physique Quantiques (UMR 5626), CNRS/Université de Toulouse 3 (Paul Sabatier), 118 route de Narbonne, F−31062 Toulouse, France

[#]Theoretical Chemistry and Biology, School of Biotechnology, Royal Institute of Technology, AlbaNova University Center, S-10691 Stockholm, Sweden

[▽]National Center for Biomolecular Research, Faculty of Science, Masaryk University, Kamenice 5/A4, CZ−62500 Brno, Czech Republic

[○]Centre for Theoretical and Computational Chemistry, Department of Chemistry, University of Tromsø—The Arctic University of Norway, N-9037 Tromsø, Norway

Supporting Information

ABSTRACT: We present new insight into the nature of aromaticity in metal clusters. We give computational arguments in favor of using the ring-current model over local indices, such as nucleus independent chemical shifts, for the determination of the *magnetic* aromaticity. Two approaches for estimating magnetically induced ring currents are employed for this purpose, one based on the quantum theory of atoms in molecules (QTAIM) and the other where magnetically induced current densities (MICD) are explicitly calculated. We show that the two-zone aromaticity/antiaromaticity of a number of 3d metallic clusters (Sc_3^-, Cu_3^+, and Cu_4^{2-}) can be explained using the QTAIM-based magnetizabilities. The reliability of the calculated atomic and bond magnetizabilities of the metallic clusters are verified by comparison with MICD computed at the multiconfiguration self-consistent field (MCSCF) and density functional levels of theory. Integrated MCSCF current strength susceptibilities as well as a visual analysis of the calculated current densities confirm the interpretations based on the QTAIM magnetizabilities. In view of the new findings, we suggest a simple explanation based on classical electromagnetic theory to explain the anomalous magnetic shielding in different transition metal clusters. Our results suggest that the nature of magnetic aromaticity/antiaromaticity in transition-metal clusters should be assessed more carefully based on global indices.

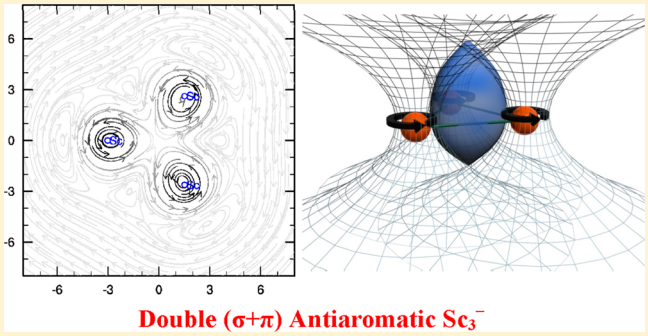

1. INTRODUCTION

The term all-metal aromaticity was introduced by Wang et al. after the discovery of an Al_4^{2-} cluster in 2001, in order to explain its exceptional gas-phase stability.[1] After this important finding, numerous theoretical and experimental studies appeared, addressing different aspects of the chemistry of all-metal aromatic/antiaromatic clusters of both main-group (MG) and transition metals (TM).[2] The chemical community was quickly intrigued by the fascinating features of this new class of molecules, such as their multiple aromaticity, that is their simultaneous and even conflicting σ, π, δ, and φ aromaticity/antiaromaticity.[2b,c,g,3,4] The aromatic nature of this new class of compounds has been exclusively studied using electronic and magnetic criteria. Applications of energetic or structural criteria are limited because it is difficult to decide on proper reference systems.[1,2,5]

However, some issues regarding the magnetic aromaticity of certain all-TM clusters have remained unclear. In particular, the patterns of nucleus-independent chemical shift (NICS) scans[6]—that is, the magnitude of the NICS[7] values at different heights above the molecular ring plane—are not consistent

Received: July 1, 2013
Published: October 14, 2013

   dx.doi.org/10.1021/ct4007184 | J. Chem. Theory Comput. 2013, 9, 4789−4796

with the proposed magnetic aromaticity for many TM clusters.[5b,f] In the present work, we explain the above-mentioned discrepancies in the light of recent advances in the analysis of the current density using the bond magnetizability approach.[8] Systems containing transition metals are known to exhibit significant nondynamical correlation effects due to the presence of closely spaced *n*d, (*n* + 1)s, and (*n* + 1)p orbitals having variable occupancies. A recent study by Pathak et al.[9] demonstrated that nondynamical electron correlation substantially affects magnetic properties of molecules with degenerate or near-degenerate ground states. It was in particular shown that the inclusion of nondynamical correlation effects can even reverse the picture obtained from a single-reference theory with respect to diatropicity or paratropicity of such systems. Accordingly, DFT results should not be blindly trusted for systems with an inherent multireference character, unless a genuine multiconfigurational theory confirms their legitimacy. We corroborate our QTAIM findings with the calculation of magnetically induced current densities (MICD) at the multiconfigurational self-consistent field (MCSCF) level of theory.[9] We reinvestigate the aromatic characters of three TM clusters from the 3d block (Sc_3^-, Cu_3^+, and Cu_4^{2-}). These state-of-the-art computations provide new insight into the aromatic nature of the investigated TM clusters that have until now not been accessible to reliable calculations.

The manuscript is organized as follows. In section 2, the computational methods used are described, and in section 3, a brief overview of previous findings as well as new results are presented and discussed for each of the clusters. Final conclusions are drawn in section 4.

2. COMPUTATIONAL METHODS

All geometries were first optimized at the density functional theory (DFT) level using the B3LYP[10] hybrid GGA exchange-correlation functional and the 6-311+G(d) basis set, as this has recently been shown to be sufficient for NICS calculations for this group of metal clusters.[5f] Frequency calculations were performed to confirm that the structures correspond to local minima. As has been reported previously,[5f] the Cu_4^{2-} cluster is a saddle point at the B3LYP/6-311+G(d) computational level, and for this reason the def2-QZVP[11] basis set was also employed to optimize the Cu_4^{2-} cluster since the D_{4h} Cu_4^{2-} is a local minimum at the B3LYP/def2-QZVP level of theory. In case of Cu_4^{2-}, two sodium salts of the cluster (C_{4v} $NaCu_4^-$ and D_{4h} Na_2Cu_4) were also optimized at the same level of theory because it is a well-known fact that doubly charged molecules are prone to spontaneous electron emission. Magnetic response properties of each cluster were computed at the same computational levels using gauge including atomic orbitals (GIAOs).[12] Since canonical molecular orbital (CMO) NICS[13] values for Sc_3^- and Cu_3^+ have not been reported previously in the literature, their CMO−NICS values were computed at the B3LYP/6-311+G(d) level in order to investigate if any valuable information can be derived from CMO−NICS values. The Gaussian 09 suite of programs was employed in these calculations.[14]

Intra- and interatomic magnetizabilities within the context of quantum theory of atoms in molecules (QTAIM)[15] were computed for the DFT-based electron densities. The contribution of each individual molecular orbital to the intra- and interatomic magnetizabilities were computed as described in ref 8. The accuracy of the calculations was controlled by keeping the atomic integral of the one-electron density Laplacian below 10^{-4} a.u. and the total energy difference between the QTAIM and DFT calculations below 0.5 kcal/mol. All QTAIM computations were performed employing the Proaim integration method, as implemented in the AIMAll suite of programs.[16]

In order to evaluate the validity of the DFT computations, magnetically induced current densities (MICD) of the different clusters were plotted at the Hartree−Fock self-consistent field (HF−SCF), DFT (B3LYP), and complete active space self-consistent field (CASSCF) levels of theory using a def2-TZVP basis set and the preoptimized geometries obtained using the B3LYP/6-311+G(d) (for Cu_4^{2-} at the B3LYP/def2-QZVP) level with a development version of the Dalton 2011 package.[17] The calculated current density plots were visualized using PyNGL.[18]

The choice of active space for any system involving transition metals is a nontrivial task and warrants careful analysis in order to achieve convergence as well as include the right amount of correlation. The obvious choice would be to include all 3d, 4s, and 4p orbitals and all the electrons therein. However, this choice (10 electrons in 27 orbitals in case of Sc_3^-) was out of reach with the available MCSCF implementation. Thus, we chose a viable active space of 10 electrons in 11 orbitals after a thorough analysis of the occupancies of natural orbitals from an MP2 calculation for Sc_3^-. The choice of active space in the case of Cu_3^+ is simpler considering that Cu has a completely filled 3d level. It can be safely concluded that the ideal choice in the case of Cu_3^+ would be two electrons in all the 4s and 4p orbitals, 12 for three Cu atoms. We brought this down to five orbitals after analyzing MP2 natural orbital occupancies. Finally, for Cu_4^{2-}, similar to Cu_3^+, the choice of active space was restricted to 6 and 12 of the 16 4s and 4p orbitals and the six electrons contained by them.

The flux of the current density was integrated on a 2D plane, perpendicular to the molecular ring plane using a Gauss−Lobatto quadrature grid, as described in ref 9. The integrated ring current strength susceptibility, referred to as current strength hereafter, provides quantitative information regarding the degree of aromaticity of a molecule as shown in various studies.[19] The sign and magnitude of the calculated ring currents provide quantitative information on the aromatic, antiaromatic, or nonaromatic character of a molecule resulting in diatropic, paratropic, or vanishing net ring currents.[20] The current strength for benzene lies between 11.8 nA/T (B3LYP/def2-TZVP) and 13.5 nA/T (CASSCF/aug-cc-pVDZ), which can be used as a reference value.

NICS can be calculated with any code providing magnetic shielding constants. The DALTON 2011 package,[16] with its implementation of GIAO−CASSCF shielding constants, provides an excellent platform for the determination of NICS values at the CASSCF−GIAO level. In this study, we report the four most commonly reported NICS indices, namely, $NICS(0)_{iso}$, $NICS(0)_{zz}$, $NICS(1)_{iso}$, and $NICS(1)_{zz}$. It is important to note here the differences in convention when comparing results from the NICS, bond magnetizability, and MICD values. Negative NICS and bond magnetizabilities denote aromatic character, whereas positive ones denote antiaromaticity. In contrast, a positive MICD value indicates an aromatic, whereas a negative MICD deontes an antiaromatic character. The plots of the current densities are interpreted as being aromatic if they are clockwise and antiaromatic if they are anticlockwise. Negative atomic magnetizabilities denote the

presence of net local diatropic currents, and positive values point to paratropic currents.

3. RESULTS AND DISCUSSIONS

Sc_3^-. Sc_3^- was proposed as a double ($\sigma + \pi$) aromatic system based on the large negative $NICS_{iso}$ values both at the center and 1 Å above the center of the molecule at the DFT (B3LYP/6-311+G(d)) computational level by Chi and Liu.[21] Later, it was suggested to be a double ($\sigma + \delta$) aromatic species.[5b] However, the $NICS_{zz}$ scan of the molecule (Figure S1) has the characteristics of neither π- nor δ-aromatic systems, because approximately at 1 Å above the ring plane, where the π- and δ-electron density increases, the $NICS_{zz}$ values become positive, indicating antiaromaticity[5b,f] which is in contrast to this conclusion.[21] An inspection of the contribution of individual MOs of the molecule to the NICS values reveals that π orbitals are fully paratropic, whereas the contribution from the σ orbitals changes when varying the height above the ring plane of the NICS probes (see Figure 1 and Table S1).

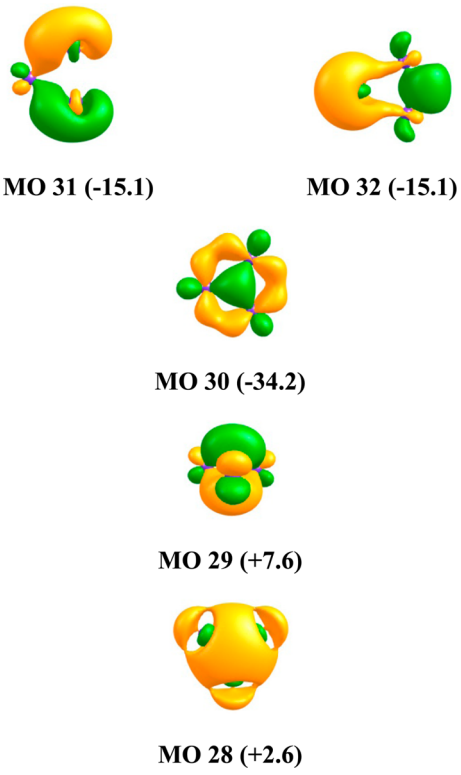

Figure 1. Visualization of canonical molecular orbitals of Sc_3^- and their contributions to $NICS(0)MO_{zz}$ in parentheses (in ppm). Note that $NICS(1)MO_{zz}$ and $NICS(2)MO_{zz}$ values (see Table S1) differ dramatically from $NICS(0)MO_{zz}$ values. Unfortunately, single-point CMO-NICS values cannot be easily decoded in terms of local currents.

Although NICS is popular, it has been shown that it sometimes fails due to factors such as local electron density[5e,22] and ring size,[5a] but none of these factors explain the unusual NICS scan patterns. Tsipis et al. suggested that the positive NICS region originates from $1e \rightarrow 2e$ allowed electronic transitions between occupied valence and virtual MOs, but it is not clear why paratropicity dominates over diatropicity in distant regions.

In order to put this problem into perspective, the magnetizability of atomic basins as well as the inter-atomic surfaces of the molecule has been investigated within the context of QTAIM. The out-of-plane interatomic magnetizability, $\chi_{ZZ}(\Omega|\Omega')$, is a reliable measure of the flux of the current density passing through the interatomic surface of the molecules. This approach is essentially similar to the gauge-including magnetically induced current (GIMIC) method proposed by Jusélius et al.,[23] but $\chi_{ZZ}(\Omega|\Omega')$ is computed for a plane defined within the context of QTAIM as the atomic boundary.

Surveying the magnetizability values reveals that both intra- and interatomic magnetizabilities of Sc_3^- are large and positive. This reflects the paratropicity of both local currents, for the atomic contribution $\chi_{ZZ}(Sc)$ and the ring current, based on the $\chi_{ZZ}(Sc|Sc')$ values, in this cluster, see Table 1.

Table 1. Isotropic and out-of-Plane Intra-Atomic ($\chi_{iso}(Sc)$ and $\chi_{ZZ}(Sc)$) and Interatomic ($\chi_{iso}(Sc|Sc')$ and $\chi_{ZZ}(Sc|Sc')$) Magnetizabilities for Sc_3^- Cluster in cgs−ppm Units at the B3LYP/6-311+G(d) Level of Theory

molecule	$\chi_{iso}(Sc)$	$\chi_{iso}(Sc\|Sc')$	$\chi_{ZZ}(Sc)$	$\chi_{ZZ}(Sc\|Sc')$
Sc_3^- (total)	+69.150	+3.477	+69.417	+2.563
Sc_3^- (MO31/32)[a]	+0.021	+0.654	+4.960	+0.991
Sc_3^- (MO30)	+54.346	+1.853	+55.104	+0.871
Sc_3^- (MO29)	+29.962	+1.682	+19.339	+2.563
Sc_3^- (MO28)	−4.629	−0.919	−4.425	−1.749
Sc_3^- (core)	−10.575	−0.448	−10.521	−1.104

[a]Contribution of each individual degenerate orbitals.

Large, positive $\chi_{ZZ}(Sc)$ values indicate the presence of very strong local electronic currents. On the other hand, based on the magnitude of $\chi_{ZZ}(Sc|Sc')$, one may classify this cluster as a *magnetically* nonaromatic to antiaromatic species. Investigating the contributions of individual MOs, obtained within the context of DFT, in the atomic and interatomic magnetizabilities demonstrates that only one MO, MO28, among the valence MOs, sustains diatropic currents, whereas the rest of the valence MOs are paratropic; the MOs are depicted in Figure 1. The conclusions drawn based on the QTAIM magnetizabilities, $\chi_{ZZ}(\Omega|\Omega')$, contradict those of previous NICS-based studies. For an unambiguous assignment of either aromatic or antiaromatic character to Sc_3^-, it is thus necessary to perform studies on magnetically induced current densities at the multiconfigurational SCF level of theory. This should ensure a proper assignment of the aromatic character and show if the use of DFT currents is appropriate for the present metal cluster. Our findings are summarized in Table 2.

The calculated magnetizability values are qualitatively in line with the integrated current strengths at the DFT and CASSCF(10,11) levels of theory. While DFT predicts significant antiaromaticity (−6.6 nA/T), the CASSCF(10,11) result borders more toward nonaromaticity, with an integrated ring current susceptibility value of −1.8 nA/T (compared with 13.5 nA/T for benzene at the CASSCF/aug-cc-pVDZ level). According to the *magnetic* criterion, Sc_3^- can be considered as a moderately antiaromatic to nonaromatic system.

The significance of nondynamical correlation for the computation of magnetic properties can also be verified by comparing the HF and CASSCF results. Whereas CASSCF computations predict a weakly net paratropic current for the molecule, HF predicts dominant diatropic currents. On the other hand, according to DFT computations, which include dynamical correlation, both the QTAIM magnetizability and

dx.doi.org/10.1021/ct4007184 | J. Chem. Theory Comput. 2013, 9, 4789−4796

Table 2. Magnetically Induced Current Densities (nA/T) and Various NICS Values in TM Clusters

clusters	computational level	MICD	$NICS(0)_{iso}$	$NICS(0)_{zz}$	$NICS(1)_{iso}$	$NICS(1)_{zz}$
Sc_3^-	HF	+2.5	−51.5	−9.5	−51.5	−2.1
	DFT (B3LYP)	−6.6	−17.5	−44.8	−21.8	+8.2
	CASSCF(10,11)	−1.8	−32.0	−31.8	−27.7	+4.1
Cu_3^+	HF	+6.3	−22.7	+1.2	−10.4	−15.0
	DFT (B3LYP)	+8.1	−28.4	−7.0	−12.2	−18.8
	CASSCF(2,5)	+6.2	−22.4	+1.5	−10.2	−14.9
Cu_4^{2-}	HF	+14.6	−12.4	−14.7	−9.5	−23.0
	DFT (B3LYP)	+15.0	−17.3	−19.7	−11.5	−25.1
	CASSCF(6,6)	+14.4	−12.6	−14.6	−9.5	−22.8
	CASSCF(6,12)	+13.8	−13.4	−14.9	−9.9	−22.9

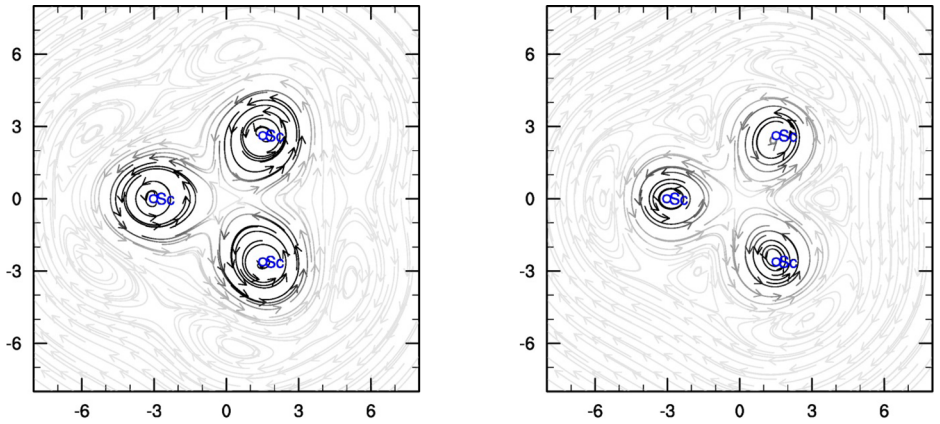

Figure 2. MICD plots for Sc_3^- at (a) B3LYP and (b) CASSCF(10,11) levels on the ring plane of the molecule. Vertical and horizontal axes represent dimensions of the space around the molecule in atomic units where the MICD is plotted. The vector arrow color intensity is proportional to the current strength. Counterclockwise vectors represent paratropic currents. Both plots show the presence of strong local paratropic currents around the scandium nuclei. HF and the intersection of DFT MICD plots are presented in Figure S2.

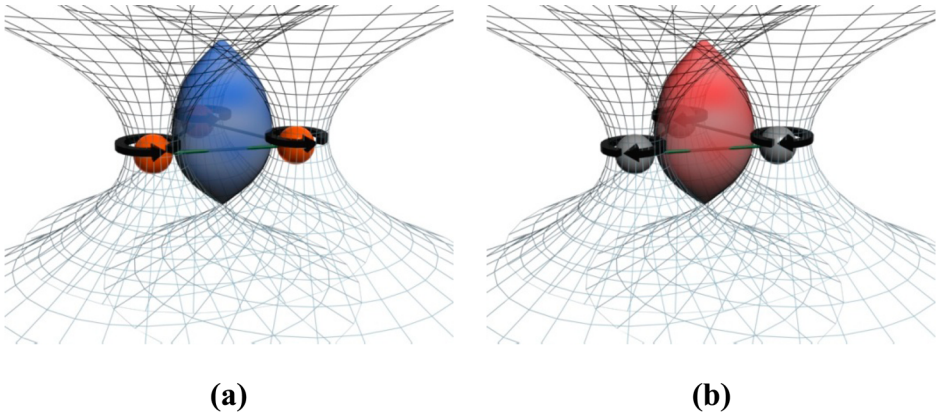

Figure 3. The influence of local electronic currents on the non-nuclear shielding values can be understood by this schematic representation. A strong local paratropic current as observed in Sc_3^- (a) induces magnetic shielding around the center of the ring in a region similar to the blue egg-shaped region in the picture. On the other hand, a strong local diatropic current as in the Cu clusters (b) induces a magnetic deshielding around the center of the ring. The red egg-shaped zone in the figure represents this deshielded zone.

the magnetically induced current strength predict a moderate antiaromaticity for Sc_3^-. Nevertheless, the aromaticity of the cluster is definitely ruled out.

MICD plots for Sc_3^- at the B3LYP and CASSCF(10,11) levels are shown in Figure 2. A notable difference between the current density plot for Sc_3^- and other molecules that have been studied in the literature so far is the presence of strong local paratropic currents around the Sc nuclei. These local currents are also clearly reflected in large positive interatomic magnetizability values (χ(Sc)).

Although the MICD and the magnetizability calculated at the DFT and CASSCF theoretical levels disprove the magnetic aromaticity of Sc_3^-, NICS(0) values are at all levels negative and consistently suggest aromaticity, see Table 2. The explanation for the large negative NICS values near the ring plane and positive values 1 Å above the ring plane could be

dx.doi.org/10.1021/ct4007184 | J. Chem. Theory Comput. 2013, 9, 4789−4796

presented in terms of a simple classical ring current model, as depicted in Figure 3.

Strong local paratropic currents around the Sc nuclei can induce large negative shielding values near the center of the molecule. Thus, it is no surprise that NICS values are negative in this region without the presence of diatropic ring currents. This explains why NICS(0) predicts an aromatic character for Sc_3^-, although the molecule is weakly antiaromatic to nonaromatic.

Cu_3^+. This cluster has been classified as a 4s, σ-aromatic molecule based on the isotropic NICS values computed by Yong et al.[5d] This is in line with the results obtained from studying the ground-state indices, i.e., orbital morphology and electron counting.[2g,5c] Later, Tsipis et al. suggested that the σ-aromaticity of the molecule is the result of both s and d atomic orbitals.[5b] However, the pattern of the out-of-plane NICS scan of the molecule is more complicated than that of a usual σ-aromatic system. An obstacle in the $NICS_{zz}$ scan of this species is the presence of a minimum zone above the ring plane (Figure S3).[5b,f] This can be verified at various theoretical levels, even in CASSCF computations, see Table 2, where $NICS(1)_{zz}$ is considerably more negative than the $NICS(0)_{zz}$. Such minimum zones are characteristic of the NICS scans of π-aromatic systems such as hydrocarbons, where weak paratropic σ-currents affect the NICS values near the ring plane.

In order to investigate the source of this probable weak σ-paratropicity, inter- and intra-atomic magnetizabilities of the molecule were computed. The magnetizabilities of the D_{3h}–Cu_3^+ cluster are listed in Table 3.

Table 3. Isotropic and out-of-Plane Intra-Atomic (χ_{iso}(Cu) and χ_{ZZ}(Cu)) and Interatomic (χ_{iso}(Cu|Cu′) and χ_{ZZ}(Cu|Cu′)) Magnetizabilities for the Cu_3^+ Cluster in cgs–ppm Units at the B3LYP/6-311+G(d) Level of Theory

molecule	χ_{iso}(Cu)	χ_{iso}(Cu|Cu′)	χ_{ZZ}(Cu)	χ_{ZZ}(Cu|Cu′)
Cu_3^+ (total)	−17.769	−2.363	−15.625	−3.917
Cu_3^+ (MO43)	−3.003	−0.983	−1.931	−1.590
Cu_3^+ (MO42)	−0.598	+0.010	−0.746	+0.043
Cu_3^+ (MO40/41)[a]	−0.645	+0.014	−0.519	+0.097
Cu_3^+ (MO38/39)[a]	−0.579	−0.079	−0.095	−0.097
Cu_3^+ (MO37)	−0.620	+0.078	−0.554	+0.258
Cu_3^+ (MO35/36)[a]	−0.643	+0.025	−0.629	+0.084
Cu_3^+ (MO33/34)[a]	−0.800	−0.120	−0.706	−0.225
Cu_3^+ (MO32)	−0.903	−0.251	−1.212	−0.605
Cu_3^+ (MO31)	−0.890	−0.160	−0.582	−0.238
Cu_3^+ (MO29/30)[a]	−0.629	−0.135	−0.749	−0.291
Cu_3^+ (MO28)	−0.639	−0.256	−0.477	−0.444
Cu_3^+ (core)	−4.525	−0.212	−4.525	−0.477

[a]Contribution of each of individual degenerate orbitals.

Evidently, both total intra- and interatomic magnetizabilities are negative, indicating the presence of the diatropic current in the cluster. Studying the contributions of individual MOs in the local and bond magnetizabilities demonstrates that the molecule mainly benefits from σ-aromaticity. The HOMO, MO43, of the cluster is the major contributor to the σ-diatropicity. This orbital is responsible for ∼41% of the total out-of-plane bond magnetizability. On the other hand, the contributions of the π-type MOs in the out-of-plane bond magnetizability are relatively small (less than 3% of the total bond magnetizability). The rest of the bond magnetizability originates from the other σ-type orbitals, namely, MO32 and MO28, Figure S4.

Interestingly, paratropicity originates from π- and δ-type orbitals (MOs 35, 36, 37, 40, and 41). The only source of σ-paratropicity in this cluster is MO42, which has a negligible paratropic contribution. However, the magnetizability computations demonstrate that local currents around the Cu nuclei are much stronger than the ring current. Accordingly, one may expect that these local currents affect the total magnetic properties more than the ring current, as is usual among the aromatic main group element (MG) clusters or molecules, as was also the case for Sc_3^-. Indeed, the minimum in the $NICS_{zz}$ scan can be interpreted in terms of an induced deshielding caused by these local electronic currents, as shown in Figure 3.

In this cluster just like for Sc_3^-, CMO-NICS values (Table S2) do not add new insight toward the nature of the problem. This is due to the local nature of NICS. CMO-NICS values cannot discriminate between the effects of local currents and ring currents in local shieldings.

The integrated current strengths at various levels of theory confirm the presence of a net diatropic ring current, showing that the system is aromatic according to the ring current criterion. The current strengths computed with HF and CASSCF(2,5) are about 6.2–6.3 nA/T and are about 2 nA/T smaller than that obtained with DFT. In addition, as is evident from the MICD plots, HF and CASSCF(2,5) predict stronger local diatropic currents. This may explain the more positive $NICS(0)_{zz}$ at these levels with respect to the DFT value. Nevertheless, strong diatropic local currents are present at all levels of theory, see Figure 4.

Thus, Cu_3^+ can be considered as aromatic according to the ring-current criterion although being less aromatic than benzene (CASSCF–MICD = 6.2 nA/T vs 13.5 nA/T for benzene).

Cu_4^{2-}. The presence of a minimum $NICS_{zz}$ zone above the ring plane has also been reported for another all-copper cluster, Cu_4^{2-}.[5f] The aromaticity of Cu_4^{2-} has been a controversial issue. Wannere et al. had introduced this cluster, in addition to Ag_4^{2-} and Au_4^{2-}, as the first example of a d-orbital-based aromatic species based on the CMO–NICS computations.[24] Later, Lin et al. suggested that the aromaticity of the molecule originates from the s atomic orbitals and that the molecule is a σ aromatic species based on GIMIC calculations.[2f] Apart from the s or d AO origin of aromaticity, the computed $NICS_{zz}$ values in Table 2 in the ring center and 1 Å above the center of the molecule do not follow the expected trend for a pure σ-ring current (Figure S6).[5f] In order to understand the origin of the more negative NICS values above the ring plane, the magnetizability of the molecule was studied within the context of QTAIM for the DFT electron density. The optimized structure for Cu_4^{2-} is a first–order saddle point at the B3LYP/6-311+G(d) computational level. Accordingly, we studied this species at two different computational levels, B3LYP/6-311+G(d) and B3LYP/def2–QZVP, since the cluster is a local minimum at the latter computational level. Interestingly, as has been reported in the case of NICS values,[5f] the magnetizabilities computed at both levels of theory are essentially the same, see Tables 4 and S1. This suggests that the nature of the stationary point of the D_{4h} Cu_4^{2-} cluster on its potential energy hypersurface has no effect on the magnetic properties of the system. Investigating the individual contributions of the MOs to local and bond magnetizabilities shows that none of them are significantly paratropic. However,

dx.doi.org/10.1021/ct4007184 | J. Chem. Theory Comput. 2013, 9, 4789–4796

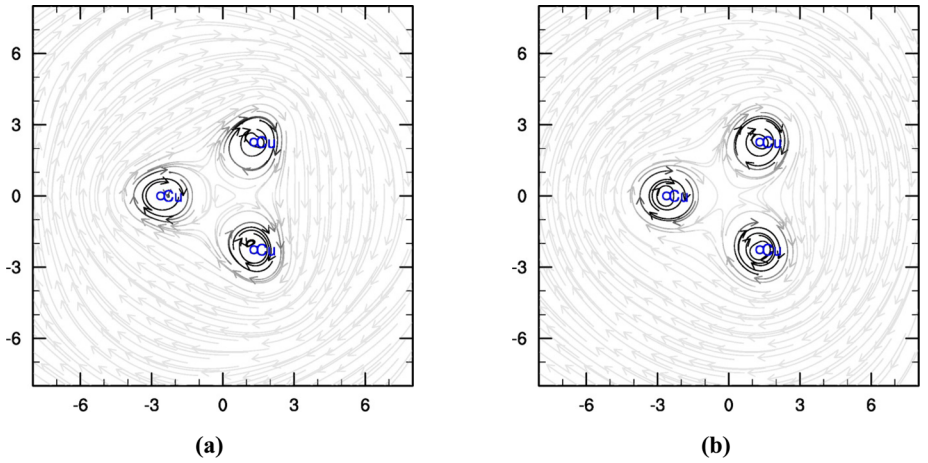

Figure 4. MICD plots for Cu_3^+ at (a) B3LYP and (b) CASSCF(2,5) levels on the ring plane of the molecule. Vertical and horizontal axes represent dimensions of the space around the molecule in atomic units where the MICD is plotted. The vector arrow color intensity is proportional to the current strength. Clockwise vectors represent diatropic currents. Both plots confirm the presence of strong local diatropic currents around the copper nuclei. A HF MICD plot is presented in Figure S5.

Table 4. Isotropic and out-of-Plane Intra-Atomic (χ_{iso}(Cu) and χ_{ZZ}(Cu)) and Interatomic (χ_{iso}(Cu|Cu′) and χ_{ZZ}(Cu|Cu′)) Magnetizabilities for the Cu_4^{2-} Cluster in cgs−ppm Units at the B3LYP/def2-QZVP Level of Theory

molecule	χ_{iso}(Cu)	χ_{iso}(Cu|Cu′)	χ_{ZZ}(Cu)	χ_{ZZ}(Cu|Cu′)
Cu_4^{2-} (total)	−26.678	−5.031	−35.780	−13.399
Cu_4^{2-} (MO58/59)[a]	−3.616	−1.156	−8.894	−4.579
Cu_4^{2-} (MO57)	−0.386	+0.133	−0.540	+0.388
Cu_4^{2-} (MO56)	−0.675	+0.110	−0.856	+0.338
Cu_4^{2-} (MO55)	−0.438	+0.246	−0.417	+0.719
Cu_4^{2-} (MO54)	−0.564	+0.036	−0.498	+0.154
Cu_4^{2-} (MO53)	−0.607	+0.091	−0.293	+0.202
Cu_4^{2-} (MO51/52)[a]	−0.468	+0.044	−0.421	+0.135
Cu_4^{2-} (MO49/50)[a]	−0.739	−0.026	−0.509	+0.155
Cu_4^{2-} (MO48)	−2.387	−0.739	−1.339	−1.336
Cu_4^{2-} (MO46/47)[a]	−0.588	−0.083	−0.782	−0.091
Cu_4^{2-} (MO44/45)[a]	−0.5575	−0.117	−0.476	−0.257
Cu_4^{2-} (MO43)	−0.692	−0.247	−0.656	−0.582
Cu_4^{2-}(MO42)	−0.859	−0.122	−0.401	−0.336
Cu_4^{2-} (MO40/41)[a]	−0.648	−0.097	−1.026	−0.162
Cu_4^{2-} (MO39)	−1.071	−0.480	−1.656	−1.061
Cu_4^{2-} (MO38)	−0.143	−0.069	+0.308	−0.150
Cu_4^{2-}(MO37)	−1.112	−0.636	−0.707	−1.192
Cu_4^{2-} (core)	−4.513	−0.486	−4.513	−0.763

[a]Contribution of each of individual degenerate orbitals.

as was the case for the Cu_3^+ cluster, considerable local diatropic currents are the reason for the relatively positive $NICS_{zz}$ values near the center of the molecule. The MICD plot in Figure 5 confirms the assumption of strong diatropic local currents. The calculated integrated current strengths agree at all levels of theory employed, ranging between 14.4 nA/T (CASSCF) and 15.0 nA/T (DFT), confirming that the molecule is more aromatic than benzene with a current strength of 11.8 nA/T (B3LYP/def2-TZVP) and 13.5 nA/T (CASSCF/aug-cc-pVDZ).

The degenerate σ-type HOMO of the Cu_4^{2-} cluster is responsible for ∼68% of the out-of-plane bond magnetizability, i.e. magnetic aromaticity. Although the contributions of these orbitals are more significant than those for the rest of the MOs, the contributions of other MOs are not negligible; the δ-type MO48 and σ-type MOs 37 and 39 are responsible for 10%, 9%, and 8% of the total bond magnetizability, respectively (see Figure S7 for MOs). It is worth mentioning that individual π-type MOs do not contribute considerably to the bond magnetizability; the sum of all contributions of π-type MOs to the bond magnetizability is also negligible. Indeed, the molecule generally benefits from σ-aromaticity in the context of magnetic aromaticity, Table 4 and Figure 5, as documented by Lin and co-workers.[2f]

Keeping in mind that many negatively charged species are prone to spontaneous electron emission,[2b,2s] we have also investigated the magnetizability of sodium salts of Cu_4^{2-} ($NaCu_4^-$ and Na_2Cu_4) to see if the nature of the local currents changes due to the presence of counterions (see Tables S4 and S5). It is evident that the relative contributions of the local currents (atomic magnetizabilities) to the ring currents (bond magnetizabilities) are very high, as was also the case for the parent compound. A notable trend in the magnetizability data is the decrease of the bond and atomic magnetizabilities when adding counterions. This decrease is mainly due to the compression of the interatomic surfaces between the copper atoms and the atomic basins of copper itself. This is clearly demonstrated in Figures S9−S14.

4. CONCLUSIONS

In this contribution, we presented magnetically induced current densities as well as QTAIM-based magnetizabilities for three prototypical 3d-TM clusters (Sc_3^-, Cu_3^+, and Cu_4^{2-}). We showed that among this group of molecules, the role of strong local electronic currents around the nuclei is non-negligible when considering the magnetic properties of the molecules. To the best of our knowledge, this phenomenon has never been observed in the case of clusters or molecules of main-group elements. It has long been known that the ring current is the major contributor to the magnetic properties of main-group molecules/clusters. Traditionally, unusual chemical shifts of substituents, attached to a molecular ring, or non-nuclear chemical shifts (computed around the ring center) have been interpreted in terms of diatropic/paratropic ring currents. Concerning this notion, large negative non-nuclear chemical shifts around the center of Sc_3^- have been interpreted as a sign of *magnetic* aromaticity of the cluster. However, careful

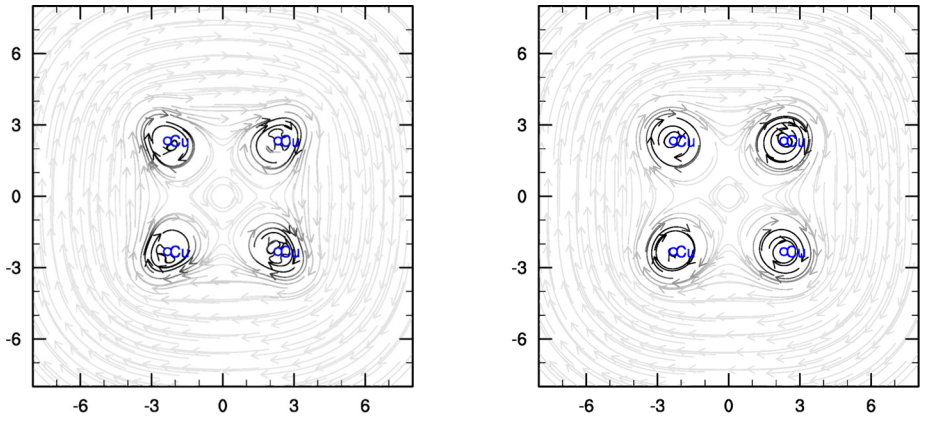

Figure 5. MICD plots for Cu_4^{2-} at (a) B3LYP and (b) CASSCF(6,12) levels in the ring plane of molecule. Vertical and horizontal axes represent dimensions of the space around the molecule in atomic units where the MICD is plotted. The vector arrow color intensity is proportional to the current strength. Clockwise vectors represent diatropic currents. Both plots confirm the presence of strong local diatropic currents around the copper nuclei. HF and CASSCF(6,6) MICD plots are presented in Figure S8.

examination of the current density by means of integrated ring current strengths using CASSCF and DFT levels of theory, as well as bond magnetizabilities, unveils the role of strong local paratropic currents. Our study shows that Sc_3^- has to be regarded as weakly antiaromatic to nonaromatic, in contrast to earlier work that predicted this molecule to be *magnetically* aromatic. Studying molecules with $NICS_{zz}$ as well as CMO-NICS scans similar to that of Sc_3^- may reveal additional molecular systems with strong local paratropic or diatropic currents. Of course, our study does not necessarily disprove aromaticity of all metallic clusters with patterns similar to that for Sc_3^-. However, these types of systems should be carefully re-examined, using QTAIM magnetizabilities as well as DFT and MCSCF current densities, when possible.

On the other side of the periodic table, exceptionally strong local diatropic currents around the copper nuclei deshield the inner space of Cu_3^+ and Cu_4^{2-} like for a typical weak paratropic ring current. The magnetic response properties of Sc_3^-, Cu_3^+, and Cu_4^{2-} in addition to a number of f-block cyclic complexes that were recently examined by Ramírez-Tagle et al.[26] highlight the significant role of local (atomic) electronic currents in the magnetic properties of this group of compounds. Finally, we point out that for the investigated TM clusters, the magnetic aromaticity does not strongly correlate with electronic, structural, or energetic criteria of aromaticity as one perhaps would expect based on the conventional notion in organic chemistry. In organic compounds, aromaticity is associated with large band gaps so that the role of nondynamic correlation effects in organic-aromatic systems is negligible.[27] In contrast, nondynamic correlation plays a crucial role among TM clusters. It is shown that the magnetic properties of Cu_4^{2-} do not change with the changing nature of this cluster on its potential energy hypersurface at different DFT levels. In addition, Sc_3^- is the global minimum on its PES,[21] and ground-state properties predict it to be aromatic; however, the magnetic criterion suggests an antiaromatic character for this species. These points indicate that the theory of aromaticity for TM clusters is still not fully understood.

The above-mentioned findings highlight a deficiency of the NICS approach. Lazzeretti discussed[28] already in 2004 that NICS is an index that estimates ring currents solely based on the information available at *one point* in the molecular space. If the ring current pattern in a molecule differs from the classical ring current pattern as seen for example for aromatic hydrocarbons,[29] then NICS cannot provide any reliable information regarding the true nature of the current density. On the basis of the above-mentioned discussion, it is highly advisible to employ current density-based approaches for studying the magnetic aromaticity of TM clusters.

■ ASSOCIATED CONTENT

Supporting Information

The morphology of MOs and additional MICD plots. This material is available free of charge via the Internet at http://pubs.acs.org.

■ AUTHOR INFORMATION

Corresponding Authors

*E-mail: ranjbar@khayam.ut.ac.ir.
*E-mail: canyslopus@yahoo.co.uk.
*E-mail: kenneth.ruud@uit.no.

Notes

The authors declare no competing financial interest.

■ ACKNOWLEDGMENTS

Z.B., P.R.-R., and C.F-N. thank Patrick Bultinck and Shant Shahbazian for their helpful discussions on an early version of this paper and Ramin Sakhtemani for his help in preparing graphics for the manuscript. This work was supported by the Program of "Emlpoyment of Newly Graduated Doctors of Science for Scientific Excellence" (grant number CZ.1.07/2.3.00/30.009) cofinanced from European Social Fund and the state budget of the Czech Republic (C.F.-N.), the project "CEITEC—Central European Institute of Technology" (CZ.1.05/1.1.00/02.0068 to R.M.) from the European Regional Development Fund, and by the Czech Science Foundation (P206/12/0539 to Z.B.). H.F. and K.R. thank the Norwegian Research Council through the CoE Centre for Theoretical and Computational Chemistry (CTCC) Grant No. 179568/V30 and the Norwegian Supercomputing Program (NOTUR) through a grant of computer time (Grant No. NN4654K). S.P. thanks the Department of Science and Technology, Govt.

of India, for his fellowship. P.R.-R. and Z.B. are grateful to the Research Council of University of Tehran for financial support. Access to the computing and storage facilities owned by parties and projects contributing to the National Grid Infrastructure MetaCentrum (Czech Republic) provided under the program "Projects of Large Infrastructure for Research, Development, and Innovations" (LM2010005) and the CERIT−SC computing and storage facilities provided under the program Center CERIT Scientific Cloud, part of the Operational Program Research and Development for Innovations, reg. no. CZ. 1.05/3.2.00/08.0144, is appreciated.

REFERENCES

(1) Li, X.; Kuznetsov, A. E.; Zhang, H. F.; Boldyrev, A. I.; Wang, L. S. *Science* **2001**, *291*, 859.

(2) (a) Kuznetsov, A. E.; Birch, K. A.; Boldyrev, A. I.; Li, X.; Zhai, H.-J.; Wang, L. S. *Science* **2003**, *300*, 622. (b) Boldyrev, A. I.; Wang, L.-S. *Chem. Rev.* **2005**, *105*, 3716. (c) Tsipis, C. A. *Coord. Chem. Rev.* **2005**, *249*, 2740. (d) Fliegl, H.; Lehtonen, O.; Lin, Y.-C.; Patzschke, M.; Sundholm, D. *Theor. Chem. Acc.* **2011**, *129*, 701. (e) Foroutan-Nejad, C.; Shahbazian, S.; Rashidi-Ranjbar, P. *Phys. Chem. Chem. Phys.* **2011**, *13*, 4576. (f) Lin, Y.-C.; Sundholm, D.; Jusélius, J.; Cui, L.-F.; Li, X.; Zhai, H. J.; Wang, L. S. *J. Phys. A* **2006**, *110*, 4244. (g) Zubarev, D. Y.; Averkiev, B. B.; Zhai, H. J.; Wang, L. S.; Boldyrev, A. I. *Phys. Chem. Chem. Phys.* **2008**, *10*, 257. (h) Foroutan-Nejad, C. *Phys. Chem. Chem. Phys.* **2012**, *14*, 9738. (i) Fowler, P. W.; Havenith, R. W. A.; Steiner, E. *Chem. Phys. Lett.* **2001**, *343*, 85. (j) Mandado, M.; Krishtal, A.; van Alsenoy, C.; Bultinck, P.; Hermida-Ramon, J. M. *J. Phys. Chem. A* **2007**, *111*, 11885. (k) *Aromaticity and Metal Clusters*; Chattaraj, P. K., Ed.; CRC Press Taylor and Francis Group: Boca Raton, FL, 2011.

(3) (a) Alexandrova, A. N.; Boldyrev, A. I.; Zhai, H.-J.; Wang, L.-S. *Coord. Chem. Rev.* **2006**, *250*, 2811. (b) Zubarev, D. Yu.; Boldyrev, A. I. *J. Comput. Chem.* **2007**, *28*, 251. (c) Galeev, T. R.; Boldyrev, A. I. *Annu. Rep. Prog. Chem., Sect. C* **2011**, *107*, 124.

(4) Tsipis, A. C.; Kefalidis, C. E.; Tsipis, C. A. *J. Am. Chem. Soc.* **2008**, *130*, 9144.

(5) (a) Foroutan-Nejad, C.; Shahbazian, S.; Feixas, F.; Rashidi-Ranjbar, P.; Solà, M. *J. Comput. Chem.* **2011**, *32*, 2422. (b) Tsipis, A. C.; Depastas, I. G.; Karagiannis, E. E.; Tsipis, C. A. *J. Comput. Chem.* **2010**, *31*, 431. (c) Feixas, F.; Matito, E.; Duran, M.; Poater, J.; Solà, M. *Theor. Chem. Acc.* **2011**, *128*, 419. (d) Yong, L.; Wu, S. D.; Chi, X. X. *Int. J. Quantum Chem.* **2007**, *107*, 722. (e) Foroutan-Nejad, C.; Badri, Z.; Shahbazian, S.; Rashidi-Ranjbar, P. *J. Phys. Chem. A* **2011**, *115*, 12708. (f) Badri, Z.; Foroutan-Nejad, C.; Rashidi-Ranjbar, P. *Phys. Chem. Chem. Phys.* **2012**, *14*, 3471.

(6) (a) Stanger, A. *J. Org. Chem.* **2006**, *71*, 883. (b) Jiménez-Halla, J. O. C.; Matitio, E.; Robles, J.; Solà, M. *J. Organomet. Chem.* **2006**, *691*, 4359.

(7) (a) Bühl, M.; van Wüllen, C. *Chem. Phys. Lett.* **1995**, *247*, 63. (b) Chen, Z.; Wannere, C. S.; Corminboeuf, C.; Puchta, R.; Schleyer, P. v. R. *Chem. Rev.* **2005**, *105*, 3842.

(8) Foroutan-Najad, C. *J. Phys. Chem. A* **2011**, *115*, 12555.

(9) Pathak, S.; Bast, R.; Ruud, K. *J. Chem. Theory Comput.* **2013**, *9*, 2189.

(10) (a) Lee, C.; Yang, W.; Parr, R. G. *Phys. Rev. B* **1988**, *37*, 785. (b) Stephens, P. J.; Devlin, F. J.; Chabalowski, C. F.; Frisch, M. J. *J. Phys. Chem.* **1994**, *98*, 11623. (c) Becke, A. D. *Phys. Rev. A* **1988**, *38*, 3098.

(11) Weigend, F.; Ahlrichs, R. *Phys. Chem. Chem. Phys.* **2005**, *7*, 3297.

(12) (a) London, F. *J. Phys. Radium* **1937**, *8*, 397. (b) McWeeny, R. *Phys. Rev.* **1962**, *126*, 1028. (c) Ditchfield, R. *Mol. Phys.* **1974**, *27*, 789. (d) Dodds, J. L.; McWeeny, R.; Sadlej, A. J. *Mol. Phys.* **1980**, *41*, 1419. (e) Wolinski, K.; Hilton, J. F.; Pulay, P. *J. Am. Chem. Soc.* **1990**, *112*, 8251. (f) Ruud, K.; Helgaker, T.; Kobayashi, R.; Jørgensen, P.; Bak, K. L.; Jensen, H. J. Aa. *J. Chem. Phys.* **1994**, *100*, 8178.

(13) Fallah-Bagher-Shaidaei, H.; Wannere, C. S.; Corminboeuf, C.; Puchta, R.; Schleyer, P. v. R. *Org. Lett.* **2006**, *8*, 863.

(14) Frisch, M. J.; Trucks, G. W.; Schlegel, H. B.; Scuseria, G. E.; Robb, M. A.; Cheeseman, J. R.; Scalmani, G.; Barone, V.; Mennucci, B.; Petersson, G. A.; Nakatsuji, H.; Caricato, M.; Li, X.; Hratchian, H. P.; Izmaylov, A. F.; Bloino, J.; Zheng, G.; Sonnenberg, J. L.; Hada, M.; Ehara, M.; Toyota, K.; Fukuda, R.; Hasegawa, J.; Ishida, M.; Nakajima, T.; Honda, Y.; Kitao, O.;Nakai, H.; Vreven, T.; Montgomery, J. A., Jr.; Peralta, J. E.; Ogliaro, F.; Bearpark, M.; Heyd, J. J.; Brothers, E.; Kudin, K. N.; Staroverov, V. N.; Kobayashi, R.; Normand, J.; Raghavachari, K.; Rendell, A.; Burant, J. C.; Iyengar, S. S.; Tomasi, J.; Cossi, M.; Rega, N.; Millam, J. M.; Klene, M.; Knox, J. E.; Cross, J. B.; Bakken, V.; Adamo, C.; Jaramillo, J.; Gomperts, R.; Stratmann, R. E.; Yazyev, O.; Austin, A. J.; Cammi, R.; Pomelli, C.; Ochterski, J. W.; Martin, R. L.; Morokuma, K.; Zakrzewski, V. G.; Voth, G. A.; Salvador, P.; Dannenberg, J. J.; Dapprich, S.; Daniels, A. D.; Farkas, O.; Foresman, J. B.; Ortiz, J. V.; Cioslowski, J.; Fox, D. J. *Gaussian 09*, revision A.02; Gaussian, Inc: Wallingford CT, 2009.

(15) (a) Bader, R. F. W. In *Atoms in Molecules: A Quantum Theory*; Oxford University Press: Oxford, 1990. (b) Keith, T. A.; Bader, R. F. W. *J. Chem. Phys.* **1993**, *99*, 3669. (c) Keith, T. A.; Bader, R. F. W. *Chem. Phys. Lett.* **1993**, *210*, 223. (d) Keith, T. A. In *The Quantum Theory of Atoms in Molecules: From Solid State to DNA and Drug Design*; Matta, C. F., Boyd, R. J., Eds.; Wiley−VCH: Weinheim, Germany, 2007; Chapter 3.

(16) Keith, T. A. AIMAll (version 11.02.27). http://aim.tkgristmill.com.

(17) DALTON, a molecular electronic structure program. http://www.daltonprogram.org.

(18) PyNGL, developed at the National Center for Atmospheric Research. http://www.pyngl.ucar.edu.

(19) (a) Fliegl, H.; Taubert, S.; Lehtonen, O.; Sundholm, D. *Phys. Chem. Chem. Phys.* **2011**, *13*, 20500. (b) Fliegl, H.; Lehtonen, O.; Patzschke, M.; Sundholm, D.; Lin, Y. C. *Theor. Chem. Acc.* **2011**, *129*, 701.

(20) Fliegl, H.; Sundholm, D.; Taubert, S.; Jusélius, J.; Klopper, W. *J. Phys. Chem. A* **2009**, *113*, 8668.

(21) Chi, X. X.; Liu, Y. *Int. J. Quantum Chem.* **2007**, *107*, 1886.

(22) (a) Foroutan-Nejad, C.; Shahbazian, S.; Rashidi-Ranjbar, P. *Phys. Chem. Chem. Phys.* **2010**, *12*, 12630. (b) Foroutan-Nejad, C.; Shahbazian, S.; Rashidi-Ranjbar, P. *Phys. Chem. Chem. Phys.* **2011**, *13*, 12655.

(23) Jusélius, J.; Sundholm, D.; Gauss, J. *J. Chem. Phys.* **2004**, *121*, 3952.

(24) Wannere, C. S.; Corminboeuf, C.; Wang, Z.-X.; Wodrich, M. D.; King, R. B.; Schleyer, P. v. R. *J. Am. Chem. Soc.* **2005**, *127*, 5701.

(25) (a) Pyykko, P.; Zhao, Y. *Mol. Phys.* **1990**, *70*, 701. (b) Pyykko, P. *Phys. Scr.* **1990**, *T33*, 52. (c) Pyykko, P.; Zhao, Y. *J. Phys. Chem.* **1990**, *94*, 7753. (d) Zubarev, D. Y.; Boldyrev, A. I. *J. Phys. Chem. A* **2008**, *112*, 7984.

(26) Ramírez-Tagle, R.; Alvarado-Soto, L.; Arratia-Perez, R.; Bast, R.; Alvarez-Thon, L. *J. Chem. Phys.* **2011**, *135*, 104506.

(27) (a) Zhou, Z.; Parr, R. G. *J. Am. Chem. Soc.* **1989**, *111*, 7371. (b) Zhou, Z.; Parr, R. G.; Garst, J. F. *Tetrahedron Lett.* **1988**, *29*, 4843.

(28) Lazzeretti, P. *Phys. Chem. Chem. Phys.* **2004**, *6*, 217.

(29) (a) Pelloni, S.; Lazzeretti, P. *J. Phys. Chem. A* **2011**, *115*, 4553. (b) Pelloni, S.; Monaco, G.; Lazzeretti, P.; Zanasi, R. *Phys. Chem. Chem. Phys.* **2011**, *13*, 20666. (c) Fliegl, H.; Sundholm, D. *J. Org. Chem.* **2012**, *77*, 3408. (d) Kaipio, M.; Patzschke, M.; Fliegl, H.; Pichierri, F.; Sundholm, D. *J. Phys. Chem. A* **2012**, *116*, 10257. (e) Fliegl, H.; Öczan, N.; Mera-Adasme, R.; Pichierri, F.; Jusélius, J.; Sundholm, D. *Mol. Phys.* **2013**, *111*, 1364. (f) Pelloni, S.; Lazzeretti, P. *J. Phys. Chem. A* **2013**, *117*, 9083.